



POLITECNICO MILANO 1863

School of Industrial and Information Engineering
Master of Science in Space Engineering

Course of Orbital Mechanics
Professor Camilla Colombo

Interplanetary trajectories and Orbit perturbations

Group ID: 2337

Last name	First name	Person code	Matriculation number
Casiero	Alessia	10691436	233125
Fiume	Elisa	10719352	243232
Gallo	Emanuele	10766758	243222
Marotta	Arianna	11015991	247719

Academic Year 2023-2024

Contents

1	Interplanetary explorer mission	1
1.1	Introduction	1
1.1.1	Constraints	1
1.2	Design Process	1
1.2.1	Preliminary analysis	1
1.2.2	Estimation of the ToFs	2
1.3	Solution methods	3
1.3.1	Genetic Algorithm	3
1.3.2	Fmincon Algorithm	3
1.3.3	Grid Search Algorithm	3
1.4	Results	3
1.5	Final trajectory characterization	4
1.6	Conclusions	5
2	Planetary explorer mission	6
2.1	Introduction	6
2.2	Orbit characterization	6
2.3	Ground Track	6
2.3.1	Repeating Ground Track	6
2.4	Orbit propagation	8
2.4.1	Cartesian coordinates	8
2.4.2	Gauss's Planetary equations	8
2.4.3	Comparison between Cartesian elements and Gauss's Planetary equations	8
2.4.4	3D perturbed orbit evolution	10
2.5	Spectral frequency analysis	10
2.6	Comparison with real data	11
	Bibliography	13
	Bibliography	13

1. Interplanetary explorer mission

1.1 Introduction

The first chapter seeks the inspection of an interplanetary explorer mission regarding three celestial bodies (departure, fly-by and target) through the exploitation of the patched conic method. The aim of the mission is to target an asteroid, Asteroid N.21 which has to be reached departing from Mercury using a powered gravity assist manoeuvre around the Earth. The solution proposed was pursued basing the calculations on the optimization of the mission cost.

1.1.1 Constraints

The assigned constraints to execute the mission are reported in the table below:

Table 1.1: Assigned specifications

Departure	Flyby	Arrival	Earliest departure	Latest arrival
Mercury	Earth	Asteroid N.21	00:00:00 01/01/2028	00:00:00 01/01/2058

Moreover, the minimum altitude of perigee for the fly-by hyperbola must be set to 200km to avoid collisions with the atmosphere of the Earth.

1.2 Design Process

1.2.1 Preliminary analysis

For our preliminary study, we opted to examine the unconstrained problem, where the constraint on the radius of perigee is not taken into account. This approach enables the observation of a diverse and wider range of scenarios that would be impractical to explore in the constrained case.

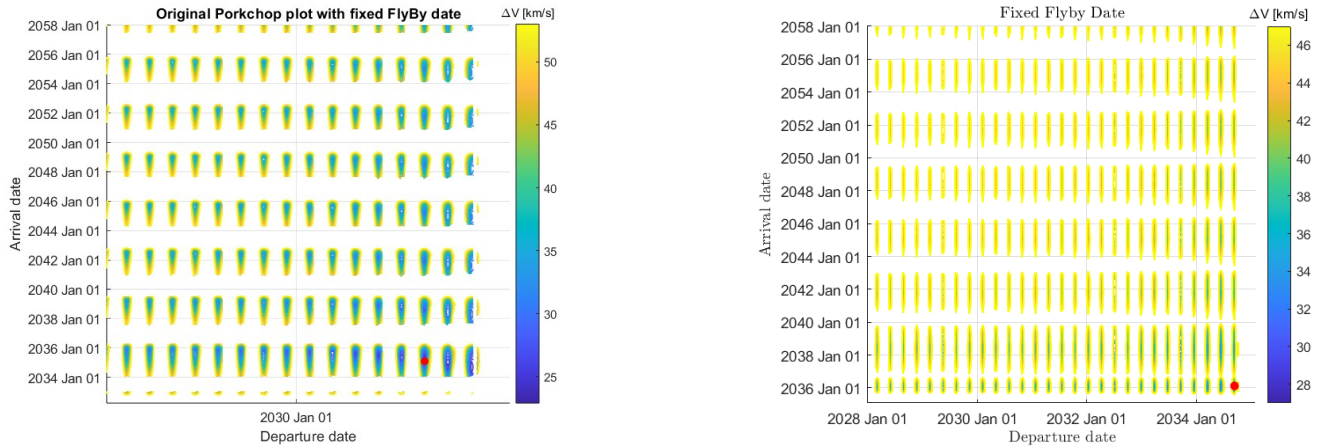


Figure 1.1: Porkchop plot with a fixed flyby date

In this context, we chose to set the position of the flyby planet, that is Earth, and analyzed a cost plot illustrating the dependency of ΔV_{tot} on the departure and arrival dates or, equivalently, on Mercury and Asteroid 21 positions. Figure (1.1) clearly shows the repeating pattern followed by ΔV_{tot} : by fixing a departure date at a minimum a new local minimum can be found at every multiple of $T_{Asteroid}$ and by fixing

the arrival date a new minimum can be found by multiples of $T_{Mercury}$, which are respectively the orbital periods of the asteroid and Mercury.

1.2.2 Estimation of the ToFs

Our conceptual approach is built upon the geometric pattern previously described. The key idea is to develop a method that constructs a grid of local minima for a meaningful number of fixed flyby dates, each with varying arrival and departure dates. To achieve this, our method identifies the initial minimum of the grid. This point is enclosed within a grid, delineated by the sum of the first departure date and the departure planet's period ($T_{Mercury}$) on the x-axis and the sum of the first arrival date and the arrival planet's period ($T_{Asteroid}$) on the y-axis. Following its localization through a grid search, we can systematically generate the coordinates of all minima points by moving from that with multiples of $T_{Mercury}$ on the x-axis and $T_{Asteroid}$ on the y-axis. The process leads to the estimation of the position of the minima as shown in Figure (1.3).

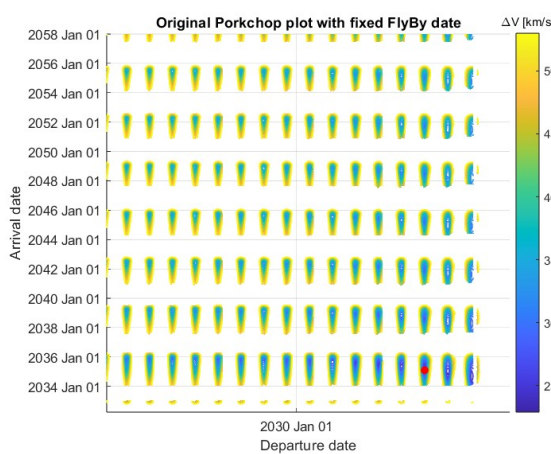


Fig. 1.2. Original Porkchop plot

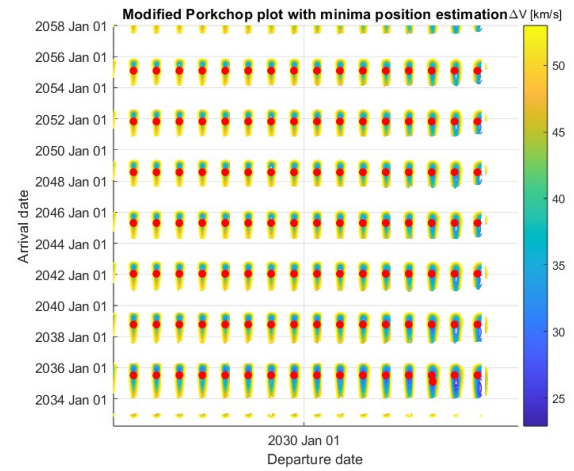


Fig. 1.3. Modified Porkchop plot

Subsequently, the (*ToFs*) were estimated through a statistical approach. Once the grid containing the positions of local minima for each of the 200 flyby dates was constructed, it became straightforward and computationally efficient to determine the position of the global minimum for each of them. This was done by using the `Dv_interplanetary_unc.m` function. This function calculates the cost in the unconstrained case under evaluations receiving as inputs the departure, flyby and arrival dates. Upon identifying these, the two *ToFs* for each minimum were computed, and a statistical analysis was conducted for each set of them. In this way, the minimum and maximum were estimated by adding and subtracting to the mean value \bar{ToF} the standard deviation σ :

$$\begin{cases} \bar{ToF}_{\min} \\ \bar{ToF}_{\max} \end{cases} = \bar{ToF} - \sigma = \bar{ToF} + \sigma$$

This procedure leads to the following (*ToFs*) boundaries:

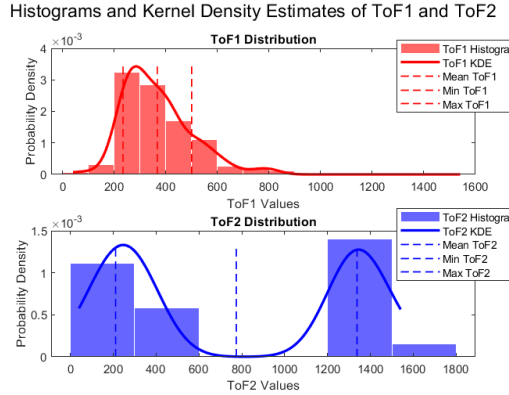


Fig. 1.4. Probability density and histogram of the ToFs

Table 1.2: ToFs boundaries

	Lower boundary	Upper boundary
ToF_1 [days]	233.788	499.971
ToF_2 [days]	211.041	1337.507

This approach facilitates defining the boundaries for the *ToFs*, serving the purpose of determining the points of minimum.

1.3 Solution methods

The optimization problem for cost introduces three degrees of freedom: the departure date from Mercury and the two *ToFs*. Following the estimation of *ToFs* through pattern recognition in the unconstrained scenario, the focus shifts towards incorporating the mission feasibility. Subsequently, the analysis employs the `Dv_interplanetary.m` function, which calculates the cost while considering constraints and the powered flyby contribution. The degrees of freedom in this phase include the departure window and the two *ToFs*.

1.3.1 Genetic Algorithm

In the initial phase, a global optimization algorithm employing the gradient method, specifically the Genetic Algorithm, was implemented using the MATLAB function `ga.m`. This algorithm seeks the minimum of a specified function while considering lower and upper boundary conditions. Given that the behaviour of the cost function did not exhibit any advantages in selecting a specific launch window, the decision was made to conduct this preliminary optimization without reducing the imposed time interval. Hence, the imposed *boundary conditions* for the *ToFs* are those detailed in Table 1.2, while for the launch windows, all dates ranging from the minimum departure to the maximum arrival are included. The critical parameters for convergence are the population size and maximum generations. Balancing computational efficiency and convergence quality, the optimal parameters are a population of 1000 and 100 maximum generations. The algorithm is executed five times ($N = 5$), improving the global minimum search, and raising confidence to 99.5%. This iterative approach, mitigating algorithmic randomness, enhances solution identification across diverse regions.

1.3.2 Fmincon Algorithm

The Matlab optimization solver `fmincon.m` was employed for a more detailed refinement of the analysis. Initializing with the value obtained from the genetic algorithm, we set boundaries by selecting dates in the neighbourhood of this value.

1.3.3 Grid Search Algorithm

The other alternative for a finer optimization was the grid search method. This consists of three nested loops that analyse all the possible combinations of departure dates and of the two *ToFs* in the neighbourhood of the optimum value found by the genetic algorithm.

1.4 Results

As it can be noticed from Table (1.3) the algorithms used for the second optimization produced slightly better results with respect to the genetic algorithm.

Table 1.3: Results

Parameter	Genetic algorithm	Fmincon algorithm	Grid Search algorithm
Total ΔV	19.1507 km/s	19.1507 km/s	19.1493 km/s
Total Time	1089.2607 days	1089.2606 days	1091.1495 days
Departure date [yyyy/mm/dd]	2039/01/23 at 19:35:19	2039/01/23 at 19:35:18	2039/01/23 at 18:51:41
Flyby Date [yyyy/mm/dd]	2040/04/13 at 15:39:55	2040/04/13 at 15:39:52	2040/04/13 at 16:38:06
Arrival date [yyyy/mm/dd]	2042/01/17 at 01:50:40	2042/01/17 at 01:50:37	2042/01/18 at 22:27:02

The best result is obtained in terms of ΔV by the grid search, at the expense of computational time. The *fmincon.m* algorithm terminated its iterations near the initial value, suggesting proximity to a local minimum. The chosen dates are the following:

Table 1.4: Choosen dates

Departure date	Flyby date	Arrival date
2039 January 23 18:51:41	2040 April 13 16:38:06	2042 January 18 22:27:02

The detailed report of the ΔV cost for each manoeuvre is shown in the following table:

Table 1.5: Cost of each manoeuvre

Manoeuvre	ΔV
Injection in the first transfer leg	15.8976 km/s
Powered gravity assist	0.0000256 km/s
Injection in the final orbit	3.2516 km/s
Total cost	19.1493 km/s

1.5 Final trajectory characterization

In Figure 1.5 the heliocentric trajectories are represented:

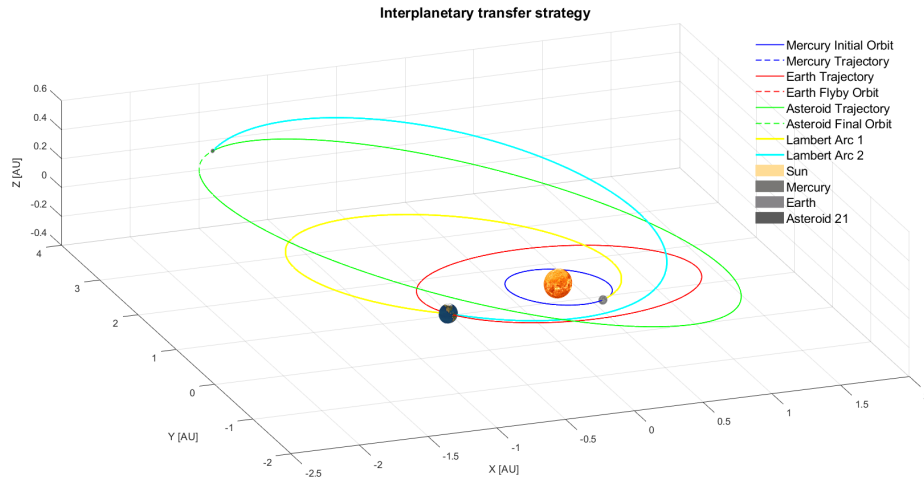


Fig. 1.5. Heliocentric trajectories

The two heliocentric transfer orbits have been computed using the Lambert solver *lambertMR.m* and can be described by the Keplerian elements reported in the table below:

Table 1.6. Keplerian coordinates

	a [km]	e [-]	i [deg]	Ω [deg]	ω [deg]	θ_i [deg]	θ_f [deg]
Lambert arc 1	$1.8284 \cdot 10^8$	0.6522	6.7289	24.3818	297.5083	339.5508	242.7690
Lambert arc 2	$2.8954 \cdot 10^8$	0.6970	9.4666	24.3818	270.7653	270.5814	189.9692

The incoming and outgoing hyperbolic trajectories are characterized by the following parameters:

Table 1.7. Parameters of the incoming and outgoing hyperbolic trajectories

	a [km]	e [-]	v_∞ [km/s]	h_p [km]	v_p [km/s]
Incoming hyperbola	-834.7118	8.8868	21.85248	212.2093	24.4668
Outgoing hyperbola	-834.7096	8.8868	21.85256	212.2093	24.4669

As it can be noticed, the constraints on the minimum altitude are respected. The total duration of the flyby considering a finite SOI is:

$$\Delta t_{SOI} = 23.4773 \text{ hours} \quad (1.1)$$

It is worth noting that the ratio between the ΔV of the impulsive manoeuvre at the pericentre of the flyby and the total ΔV provided by the flyby is extremely low:

$$\frac{\Delta V_{pow}}{\Delta V_{flyby}} = 5.2 \cdot 10^{-6} \quad (1.2)$$

Where $\Delta V_{flyby} = 4.91795 \text{ [km/s]}$ The hyperbolic trajectories are represented in Figure (1.6).

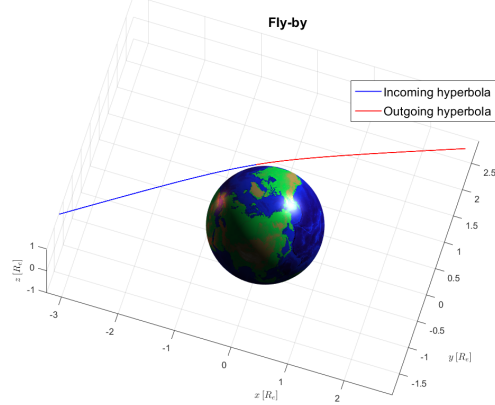


Fig. 1.6. Flyby plot

1.6 Conclusions

From Table 1.5, it is evident that the initial transfer, from Mercury to Earth, incurs the highest cost. The flyby cost is, instead, the lowest, primarily attributed to the nearly identical incoming and outgoing hyperbolas during this phase.

To further mitigate the total mission cost, the possibility of incorporating multiple flybys could be explored. This strategic utilization of flybys has the potential to optimize trajectory efficiency and minimize overall mission expenses.

2. Planetary explorer mission

2.1 Introduction

The second chapter attempts to analyze the trajectory followed by a small spacecraft by means of the propagation of Cartesian coordinates and Gauss's Planetary Equations. The mission analysis includes the contribution of two orbit perturbations: the J_2 effect and the Moon perturbation. First, ground track estimations will be conducted, then, orbit propagation and spectral analysis will be studied. In the end, a comparison with a real satellite mission will be reported.

2.2 Orbit characterization

The prescribed initial parameters are semi-major axis a_0 , eccentricity e_0 and inclination i_0 . The initial set of parameters that describes the nominal orbit used for planetary explorer mission study is:

Table 2.1. Initial Keplerian coordinates

a [km]	e [-]	i [deg]	Ω [deg]	ω [deg]	θ [deg]
42164	0.0007	0.1378	0	0	40

The orbit period is $T = 86119,94\text{s}$, which is similar to the period of a geosynchronous orbit, moreover, being the inclination almost null, the orbit is almost geostationary. The perturbation related to J_2 effect is due to the oblateness of the Earth, which is not a perfect sphere. As a consequence, the change of direction of the gravity force arises and the gravity attraction between two bodies will depend on the latitude. The secular effect of J_2 causes a variation on Ω , ω and θ causing the nodal regression, a westward movement of the node line for the case of prograde orbit under evaluation, and the perigee precession.

$$\begin{cases} \dot{\Omega}_{sec} = -\frac{3 n R_E^2 J_2}{2 p^2} \cos i \\ \dot{\omega}_{sec} = \frac{3 n R_E^2 J_2}{4 p^2} (4 - 5 \sin^2 i) \\ \dot{M}_{sec} = -\frac{3 n R_E^2 J_2}{4 p^2} (3 \sin^2 i - 2) \end{cases} \quad (2.1)$$

On the other hand, the perturbation due to the direct gravitational attraction of the Moon on the spacecraft is particularly significant for HEO and GEO orbits. The principal effects of such a perturbation are secular changes in i , e and ω .

2.3 Ground Track

The ground track is the projection of the satellite's orbit over the Earth's surface. In order to evaluate the effects of the perturbations, both the perturbed (by means of Cartesian coordinates) and unperturbed cases have been reported in the same plot. The time evolution of the ground tracks is presented for one orbital period, one year and five years, time span considered relevant for the case studied.

2.3.1 Repeating Ground Track

The repeating ground track aims at the improvement of the communications between the satellite and the ground station since, due to their different velocities, the ground track would be subjected to a westward shift in terms of longitude for each period: $\Delta\lambda = T\omega_E$. To prevent this and obtain an exact repetition of the

ground track, a modification of the semi-major axis is needed, which means modifying the orbit period. The ratio k:m was given as 1:1, so that $\frac{T}{T_E} = \frac{m}{k}$. From which, the new period of the orbit, and, consequently, the semi-major axis, can be evaluated $a_{unp} = \left(\frac{\mu_E m^2}{w_E^2 k^2} \right)^{\frac{1}{3}}$. In the case of an unperturbed problem, the semi-major axis does not change over the periods. Whereas, for the perturbed motion, each orbit ground track is different from the previous one. Solving the implicit function of the secular regression of the ascending node, with the aid of the Matlab numerical algorithm *fzero*, the semi-major axis is modified:

$$\frac{m}{k} = \frac{\omega_E - \dot{\Omega}}{n + \dot{\omega} + \dot{M}} \quad (2.2)$$

Table 2.2. Semi-major axis for nominal and modified orbits

Nominal	Modified (No perturbations)	Modified (Perturbation)
a [km]	42164	42166.16656655807

The graphs offer a comparison of both the perturbed and unperturbed cases in the nominal and repeating.

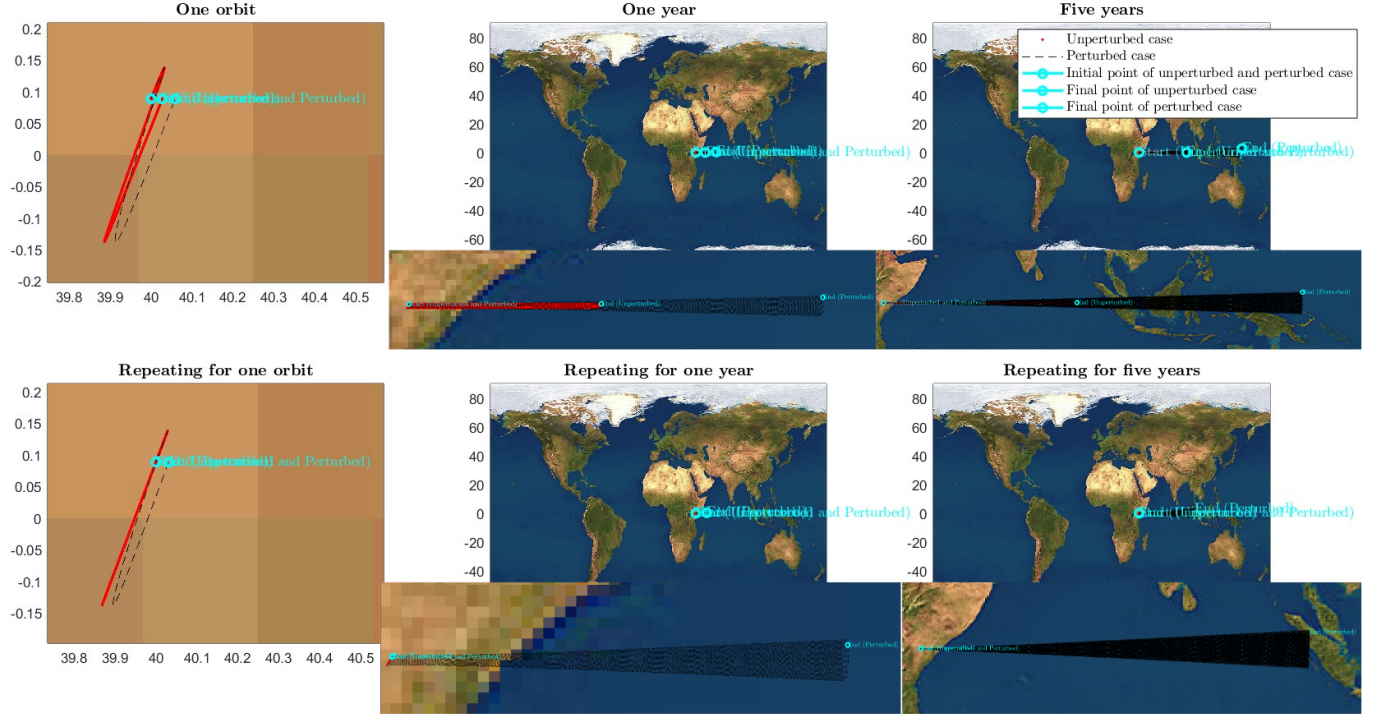


Fig. 2.1. Ground Track

Since the orbit analysed is almost geostationary, the ground track is not that variable, thus, a zoom in is required. As can be seen, enlarging the time span considered, the differences between unperturbed and perturbed case increase, since the perturbations, although small in a short period of time, sum their effects along time. It can be noted that the unperturbed case shows perfect overlap over multiple orbits. This do not happen in the perturbed case because, due to the time-dependency of the perturbations, the repeating semi-major axis should be computed at each step of propagation, thus, resulting in excessive computational effort.

2.4 Orbit propagation

The propagation of the perturbed orbit has been studied following two procedure: the integration of the Cartesian equation of motion, obtaining the state as function of position and velocity vector, $\vec{s}_{car}(t) = \{\vec{r}(t), \vec{v}(t)\}$ and the integration of the Gauss planetary equations obtaining the state as function of Keplerian elements, $\vec{s}_{Kep}(t) = \{a(t), e(t), i(t), \Omega(t), \omega(t), \theta(t)\}$.

2.4.1 Cartesian coordinates

The equation of motion to be integrated is:

$$\ddot{\vec{r}} = -\frac{\mu}{r^3} \vec{r} + \vec{a}_{J_2} + \vec{a}_{Moon} \quad (2.3)$$

Where the perturbing accelerations expressed in the Cartesian coordinates are:

$$\begin{cases} \vec{a}_{J_2} = \frac{3}{2} \left(\frac{J_2 \mu R_E^2}{r^4} \right) \left[\frac{x}{r} \left(5 \frac{z^2}{r^2} - 1 \right) \hat{i} + \frac{y}{r} \left(5 \frac{z^2}{r^2} - 1 \right) \hat{j} + \frac{z}{r} \left(5 \frac{z^2}{r^2} - 3 \right) \hat{k} \right] \\ \vec{a}_{Moon} = \mu_{Moon} \left(\frac{\vec{r}_{sc-Moon}}{r_{sc-Moon}^3} - \frac{\vec{r}_{Earth-Moon}}{r_{Earth-Moon}^3} \right) \end{cases} \quad (2.4)$$

2.4.2 Gauss's Planetary equations

The effect of perturbation on Keplerian parameters is evaluated using Gauss planetary equations (1). Although being implemented also for the TNH (or Tangential – Normal – Out-of-plane) reference frame, it was chosen to display them in the RSW (or Radial - Transversal - Out-of-plane) reference frame, evaluating the accelerations as follows:

$$\begin{cases} a_{J_2}^{RSW} = -\frac{3}{2} \frac{J_2 \mu R^2}{r^4} \begin{bmatrix} 1 - 3 \sin^2 i \sin^2(\theta + \omega) \\ \sin^2 i \sin 2(\theta + \omega) \\ \sin 2i \sin(\theta + \omega) \end{bmatrix} \\ \vec{a}_{Moon}^{RSW} = [\hat{r}, \hat{s}, \hat{w}]^T \vec{a}_{Moon}^{XYZ} \end{cases} \quad (2.5)$$

It must be noted that the moon perturbation acceleration is obtained as a transofrmation of reference system from ECI (or Earth-Centered Inertial) to RSW.

2.4.3 Comparison between Cartesian elements and Gauss's Planetary equations

To carry out the comparison between those two methods, a propagation of 500 orbits from 00:00:00 01/01/2028 is performed. The graphs below represent the evolution of the same parameters through Cartesian coordinates and Gauss's planetary equations together with a measure of error between them, properly chosen case by case. The results are shown in Figures (2.3, 2.4, 2.5):

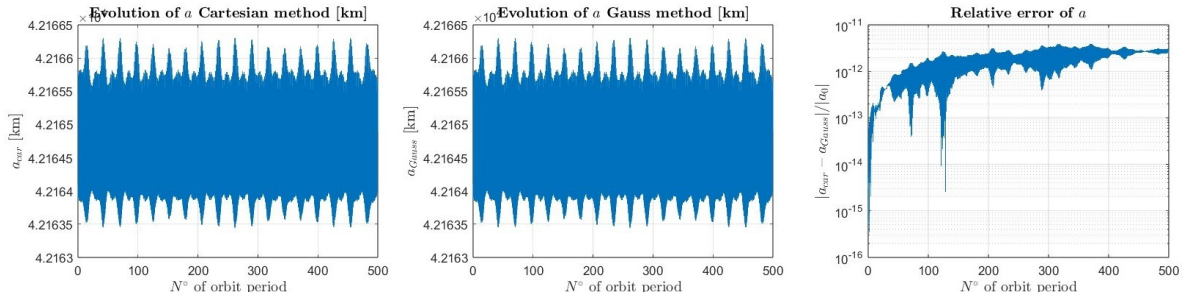


Fig. 2.2. Cartesian and Keplerian evolution of a with relative error

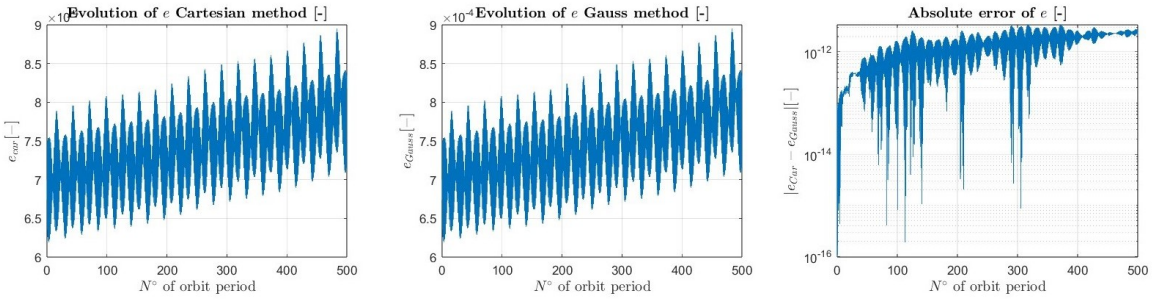


Fig. 2.3. Cartesian and Keplerian evolution of e with relative error

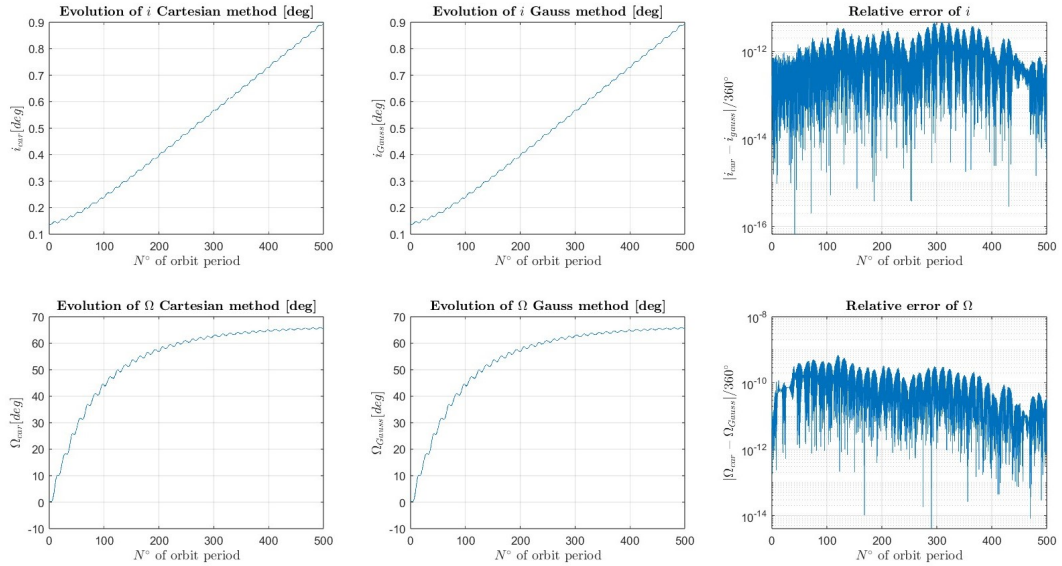


Fig. 2.4. Cartesian and Keplerian evolution of i and Ω with relative error

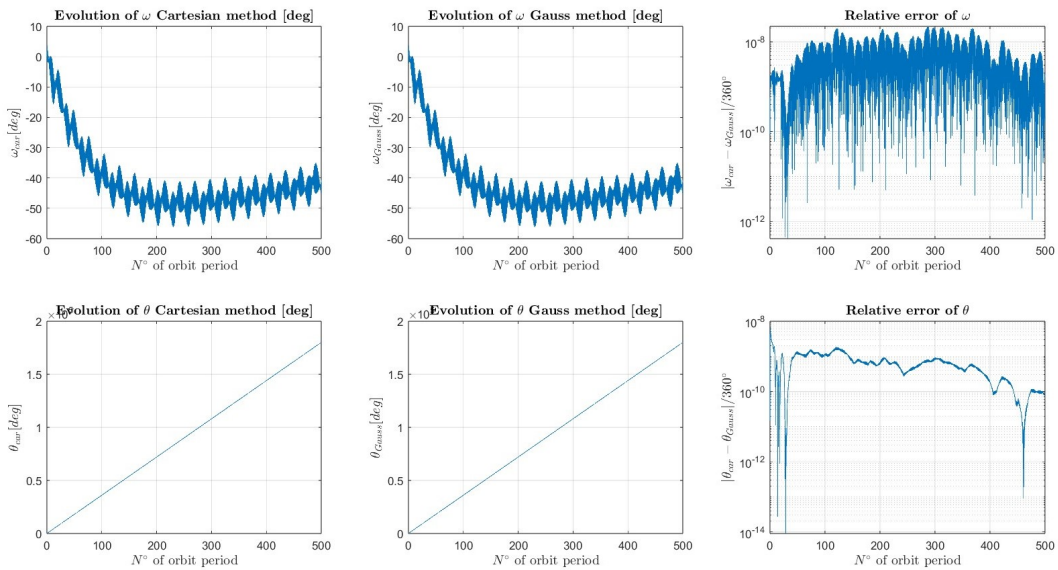


Fig. 2.5. Cartesian and Keplerian evolution of ω and θ with relative error

A further comparison between those two methods is conducted analysing the computational effort involved.

in their solution. Directly identifying the computational cost in terms of floating point operations implied could be cumbersome, so a more practical approach is used. This consists in identifying the time consumption spent by the two algorithms considered with various length of the time span assigned to the solution both by means of Cartesian coordinates and Gauss's planetary equations. The outcomes of this analysis are here depicted. As can be seen, the Gauss's planetary equations algorithm is less time consuming, thus, resulting in less computational effort with respect to the Cartesian coordinates method. Therefore, if the computational resources are limited, the former method must be preferred.

2.4.4 3D perturbed orbit evolution

The perturbed orbit evolution due to J2 effects and Moon perturbation is reported in the subsequent plot:

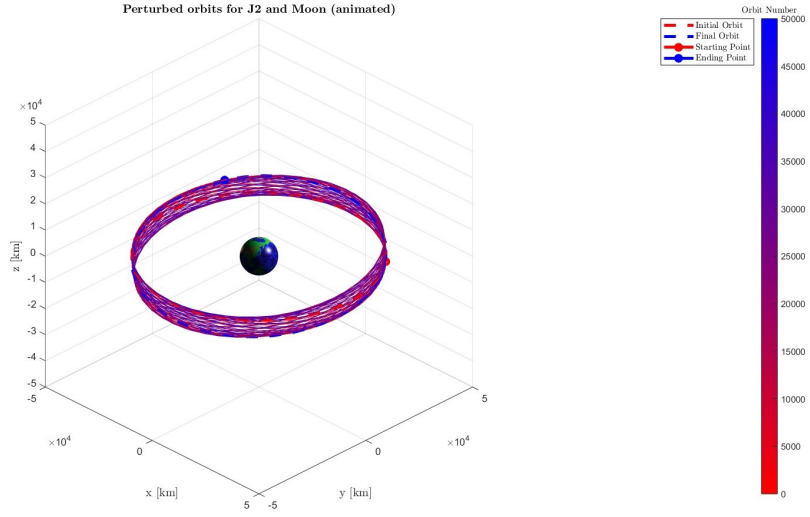


Fig. 2.7. 3D perturbed orbit evolution

2.5 Spectral frequency analysis

Orbit perturbation effects can be divided in three different types: short-period, long-period and secular. Short and long period variations will repeat the element variation pattern after a certain amount of time: less than one orbit and few orbits, respectively. Due to their periodic behaviour these variations can be neglected in a long term analysis. This can be done by filtering the results coming from the orbit propagation. To do so for the short-periodic and long-periodic oscillations, the moving-average low-pass filtering is implemented through the application of the Matlab function *movmean.m*, which computes the means at each point considering only the neighbouring values. Filtering the short-periodic oscillations in a time interval equal to one orbit, the main perturbations observed are long term oscillations and secular variation (non-periodic). Filtering for

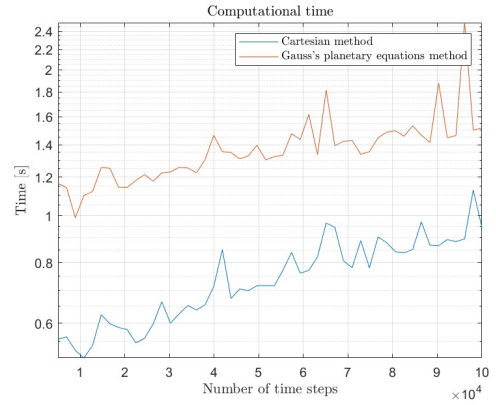


Fig. 2.6. Computational time comparison between Cartesian elements and Gauss's Planetary equations

a time period equal to $15T$, only secular variations are left. In the plot, unfiltered keplerian elements and both the filtered results appear:

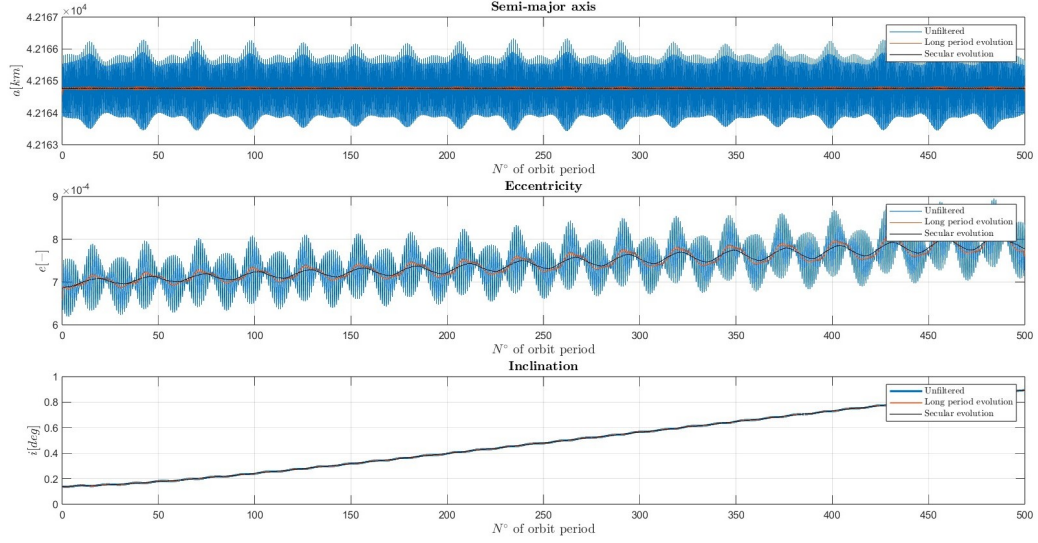


Fig. 2.8. Unfiltered and filtered evolution for a, e, i

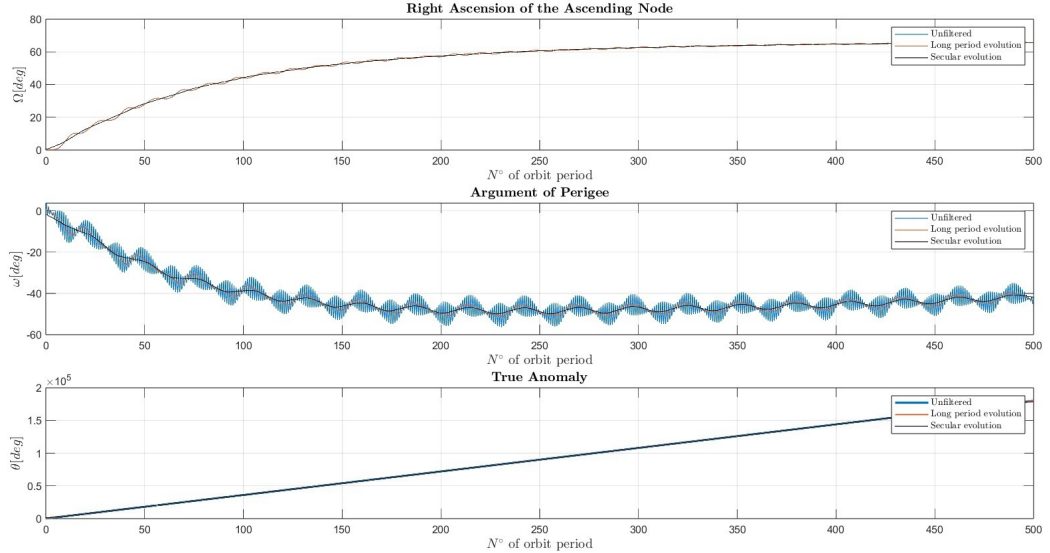


Fig. 2.9. Unfiltered and filtered evolution for Ω, ω, θ

2.6 Comparison with real data

To validate the consistency of the orbit propagation of the model studied in the present work, a comparison with real data of a real celestial object mission has been done. The satellite chosen for this aim is SKYNET 1 (NORAD Catalogue ID: 4250) with a geo-synchronous orbit with similar semi-major axis, eccentricity and inclination. Its initial Keplerian parameters as well as TLEs for the propagation have been taken from *Space – Track.org* website (2). The propagation of its orbit had been performed, using the *Nasa – Horizon.com* website (3), from an initial date of 00:00:00 28/02/2000 to a final date 00:00:00 28/02/2002

expressed in MJD2000. In the chosen time range SKYNET 1 was uncontrolled, so that the evolution of its orbital parameter is only caused by perturbations, enhancing, thus, the similarity with the case analysed. The comparison between the propagated data and the real ones obtained is the following:

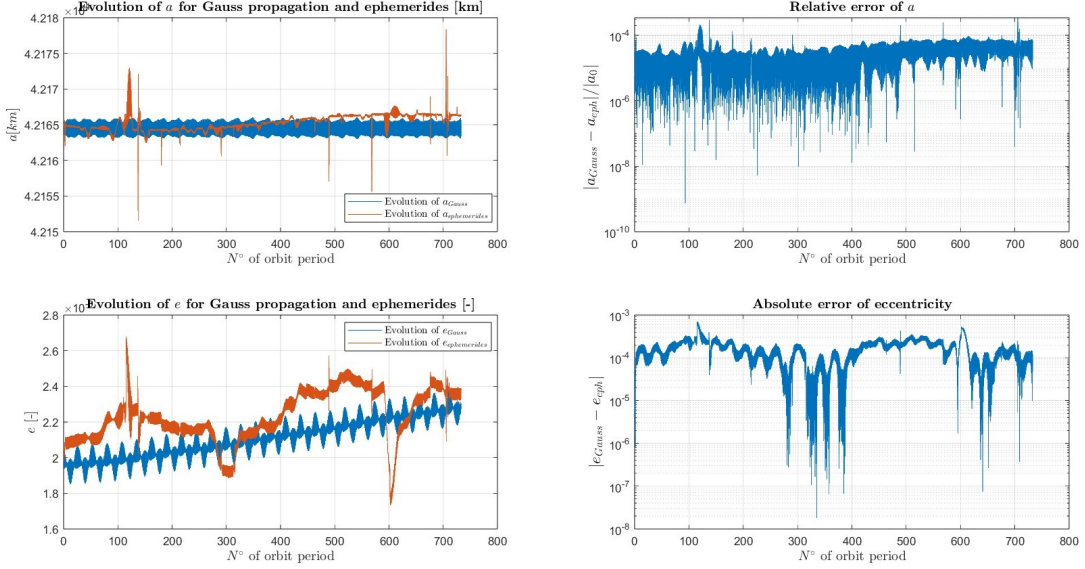


Fig. 2.10. Evolution of a and e for Gauss propagation and ephemerides with relative error

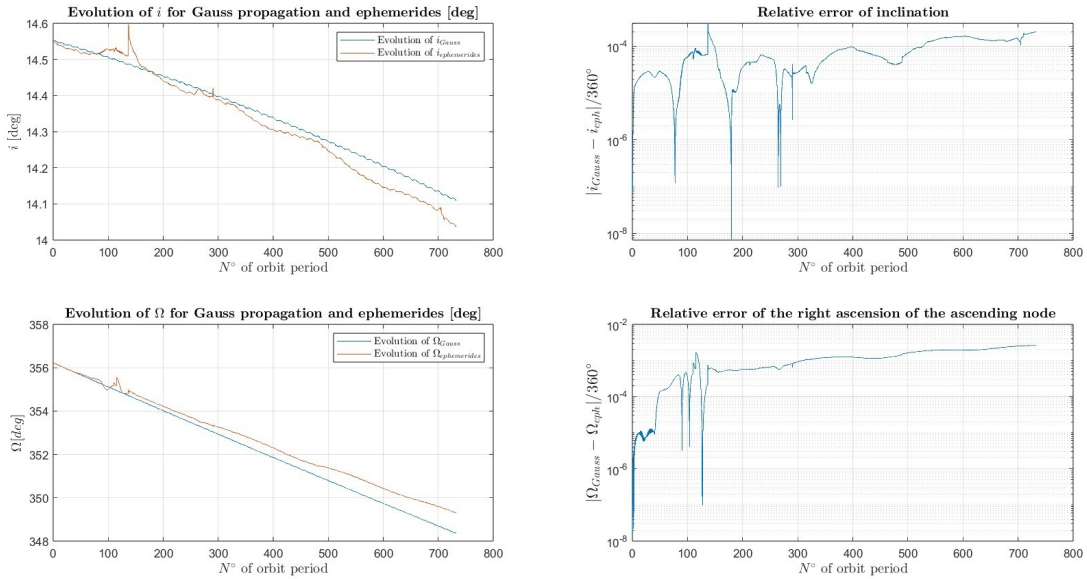


Fig. 2.11. Evolution of i and Ω for Gauss propagation and ephemerides with relative error

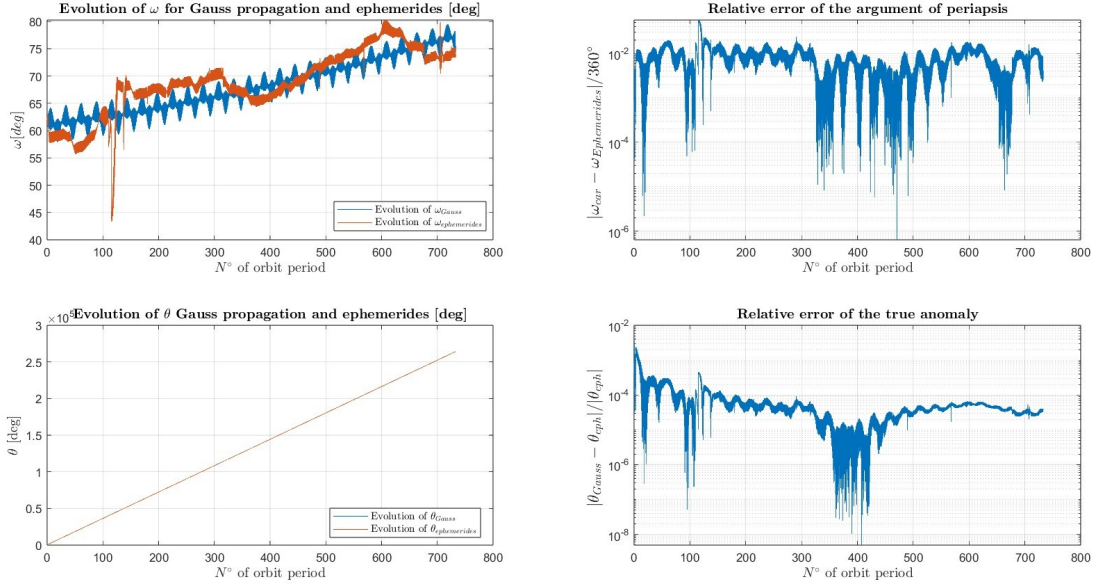


Fig. 2.12. Evolution of ω and θ for Gauss propagation and ephemerides with relative error

As can be seen from the graphs, the evolution of the Keplerian elements become slightly different from the real data during the propagation. This is due to the fact that in the present work the only perturbations considered are the J_2 effect and the Moon gravity, thus, other sources of disturbances to the nominal orbits are neglected. Other perturbations could be, for example, third-body one, higher order gravitational perturbations and solar radiation pressure. The latter could be considered particularly relevant in this real application, especially because this satellite is in high altitude earth orbit.

Bibliography

1. Richard Battin, *An Introduction to the Mathematics and Methods of Astrodynamics*, 1987
2. Space-Track.org, <https://www.space-track.org/>
3. Nasa-Horizon.com, <https://ssd.jpl.nasa.gov/horizons/app.html#/>